Peer-to-Peer Energy Transfer by Power Gyrators Based on Time-Variable-Transformer Concept

Daniel Kiss, Takashi Hisakado, *Member, IEEE*, Tohlu Matsushima, *Member, IEEE*, and Osami Wada, *Member, IEEE*

***Abstract*—A control strategy based on matching the source and load changes of the order of milliseconds, called peer-to-peer energy transfer, is introduced. This energy transfer enables a decoupled energy transfer system in common bus networks. To realize the transfer with a pair of two-port circuits, a power gyrator is derived from the phasor-based model of a bidirectional ac/dc converter, based on the concept of a time-variable transformer. Power-gyrator timing synchronization is achieved by communication, and a peer-to-peer energy transfer system is developed. Experimental and simulation results are compared, and it is demonstrated that peer-to-peer energy transfer can be used for decoupling common bus voltage networks.**

***Index Terms*—Decoupled system, peer-to-peer energy transfer, power gyrator, time-variable transformer (TVT), timing synchronization.**

I. Introduction

In recent years, microgrids have been extensively researched [1], [2] for addressing the challenges posed by the expansion of distributed generation and energy storage systems, to use them to the utmost, while improving the reliability of the legacy grid. A significant challenge in microgrid research is the determination of control strategies that are reliable, efficient, and applicable in both grid-connected and islanded modes. Most sources and batteries are connected through an inverter, with the ac side connected to a common bus, creating a network of parallel inverters.

The droop method, originally introduced in [3], is based on the operation of parallel synchronous generators because uninterruptible power supply is the most commonly used control strategy for microgrids [4]. The original droop control has been modified in several ways to accommodate the lower voltages of microgrids. Guerrero *et al.* in [5] use the P–V droop instead of the traditional P–ω droop; in [6] they use a virtual inductance to lower the line resistance (R)/inductance (X) ratio, whereas Li *et al.* [7] modify the reference frame for adjusting to any R/X value. For improving the inertia of droop-controlled systems, a swing equation [8], [9] has been introduced, which mimics not only the steady state but also the transient behavior of synchronous generators. Droop control is generally implemented in individual inverters, rendering it the primary level of control. A secondary level of control is necessary for maintaining the frequency and voltage [10], and for sharing the reactive [11] [12], harmonic, and unbalanced power [13], [14]. Approaches with [10], [11], [13] and without [12], [14] communication exist for these purposes. Nondroop-based approaches have also been garnering attention, of late; for example, the implementation of virtual oscillators [15] or consensus-based [16] methods.

Although most of the above-mentioned approaches ignore the inherent communication delays in these systems, studies dealing with communication delays have been reported recently [2]. To adjust the reference signals in the secondary control, gain scheduler methods are utilized for decreasing the influence on the delays [17]. In [18], the effects of the delays are analyzed and in [19] and [20], the delays are estimated using a Smith predictor for delay prediction or a model-predictive-control approach [21]. Further, distributed coordinated controls are reported in [16], [22], and [23]. In most of the current approaches, the delays in the control system for the secondary level are considered; however, the sources and loads do not coordinate with each other to maintain network reliability in the short time scale.

In peer-to-peer energy transfer, every network member is connected to a common ac bus and two network members match their changes in the order of milliseconds; hence, these changes have no effect on the common bus voltage. Although the network is coupled through the common voltage, by matching the changes, they can be decoupled from the rest of the network. A peer-to-peer energy transfer system with time-variable phasors is formulated and realized using bidirectional ac/dc converters. The converter is modeled, using the time-variable transformer (TVT) concept [24] and a gyrator, applicable in power processing is derived [25].

Gyrators change the characteristics of the connected one-port circuit to its dual, i.e., they change the battery characteristic, which is similar to a voltage source, to a characteristic that is

Manuscript received August 3, 2018; revised October 25, 2018; accepted November 8, 2018. Date of publication November 19, 2018; date of current version May 22, 2019. This work was supported in part by JST, CREST and Grants-in-Aid for Scientific Research under Grant 24560456. Recommended for publication by Associate Editor A. Davoudi. *(Corresponding author: Takashi Hisakado.)*

D. Kiss was with the Department of Electrical Engineering, Graduate School of Engineering, Kyoto University, Kyoto 615-8510, Japan (e-mail: kissda@gmail.com).

T. Hisakado and O. Wada are with the Department of Electrical Engineering, Graduate School of Engineering, Kyoto University, Kyoto 615-8510, Japan (e-mail: hisakado@kuee.kyoto-u.ac.jp; wada@kuee.kyoto-u.ac.jp).

T. Matsushima was with the Department of Electrical Engineering, Graduate School of Engineering, Kyoto University, Kyoto 615-8510 Japan. He is now with the Department of Electrical and Electronic Engineering, Kyushu Institute of Technology, Kitakyushu 804-8550, Japan (e-mail: matsushima@ele.kyutech.ac.jp).

Color versions of one or more of the figures in this paper are available online at http://ieeexplore.ieee.org.

Digital Object Identifier 10.1109/TPEL.2018.2882129

0885-8993 © 2018 IEEE. Translations and content mining are permitted for academic research only. Personal use is also permitted, but republication/redistribution requires IEEE permission. See http://www.ieee.org/publications_standards/publications/rights/index.html for more information.

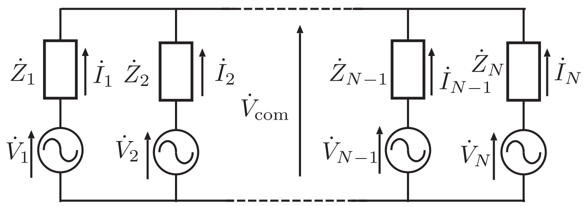

Fig. 1. Model of the peer-to-peer energy transfer system using variable voltage sources. Each network member, which is a source or load, is represented by its Thevenin equivalent circuit. The voltage phasors change in discrete time.

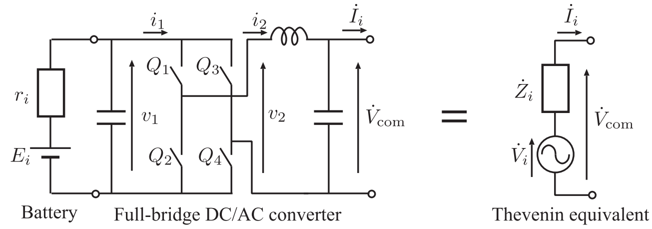

Fig. 2. Each member of the peer-to-peer energy transfer in Fig. 1 consists of dc battery and full-bridge ac/dc converter. The converter is modeled by a two-port network and the dc battery is modeled by voltage source E_i and internal resistance r_i.

more similar to a current source. Thereby, they act as current sources, and are not considerably affected by the changes in the bus voltage, rendering them suitable for peer-to-peer energy transfer. Further, timing synchronization is introduced between the converters by communication and energy-transfer matching, in the order of milliseconds, is realized.

The remainder of this paper is organized as follows. In Section II, the peer-to-peer energy transfer system is described in detail. In Section III, a phasor-based model of the bidirectional ac/dc converter is presented. In Section IV, the realization of the gyrator using voltage–current hybrid control is described. In Section V, the converter used in our experiments is presented. In Section VI, our experimental and modeling results are presented, and in Section VII, the conclusions are drawn.

II. Peer-to-Peer Energy Transfer

The peer-to-peer energy transfer system is a network of variable voltage sources with internal impedances, which are the Thevenin equivalent circuits of sources and loads connected in a star architecture, as shown in Fig. 1. The voltage sources are synchronized such that their output current has the same phase as the voltage at the point of common coupling, making the power factor unity. As observed in [26] and [27], a system sampled with the ac frequency is a good approximation of the actual operation. In this case, the system can be described by phasors that are discretized in time. This system can be described as follows:

$$\dot{V}_{\text{com}}(k) = \dot{V}_i(k) - \dot{Z}_i\dot{I}_i(k), \quad \text{where} \quad i = 1, 2, ..., N \tag{1}$$

and

$$\dot{V}_{\text{com}}(k) = \frac{\sum_{i=1}^{N} \frac{\dot{V}_i(k)}{\dot{Z}_i}}{\sum_{i=1}^{N} \frac{1}{\dot{Z}_i}} \tag{2}$$

where k is the sampled moment in time, $\dot{V}_{\text{com}}(k)$ is the voltage at the common point at time k, $\dot{V}_i(k)$ is the voltage of the ith ideal voltage source, and $\dot{Z}_i$ is the internal impedance. From (2), the coupling coefficient γ_i, which shows the effect of $\dot{V}_i$ on $\dot{V}_{\text{com}}$, can be derived as

$$\dot{V}_{\text{com}}(k) = \sum_{i=1}^{N} \gamma_i \dot{V}_i(k), \quad \text{where} \quad \gamma_i = \frac{\frac{1}{\dot{Z}_i}}{\sum_{i=1}^{N} \frac{1}{\dot{Z}_i}}. \tag{3}$$

Assume that the next voltage $\dot{V}_i(k+1)$ of each member of the network depends only on $\dot{V}_i(k)$ and $\dot{V}_{\text{com}}(k)$, then

$$\dot{V}_i(k+1) = f_i(\dot{V}_i(k), \dot{V}_{\text{com}}(k)), \quad \text{where} \quad i = 1, 2, ..., N \tag{4}$$

and there is at least one steady state where if $\dot{V}_{\text{com}}(k)$ does not change, the voltages of the modules also do not change. The steady state is denoted by an upper index "SS." Then

$$\begin{aligned} &\dot{V}_i^{\text{SS}}(k+1) = \dot{V}_i^{\text{SS}}(k), \\ &\text{if } \dot{V}_{\text{com}}^{\text{SS}}(k+1) = \dot{V}_{\text{com}}^{\text{SS}}(k),\ i = 1, 2, ..., N. \end{aligned} \tag{5}$$

Assume that the system is in the steady state. Then, two voltage sources of the network are selected with voltages $\dot{V}_1$ and $\dot{V}_2$, and their voltages are changed by $\Delta\dot{V}_1$ and $\Delta\dot{V}_2$, respectively. Using the coupling coefficients from (3), we obtain

$$\Delta\dot{V}_{\text{com}}(k) = \gamma_1\Delta\dot{V}_1 + \gamma_2\Delta\dot{V}_2 \tag{6}$$

where $\Delta\dot{V}_{\text{com}}(k)$ is the deviation from the steady-state common point voltage $\dot{V}_{\text{com}}^{\text{SS}}(k)$. From (5), if $\Delta\dot{V}_{\text{com}}(k) = 0$, the rest of the system remains unaffected. To satisfy this condition

$$\frac{\Delta\dot{V}_1(k)}{\dot{Z}_1} = -\frac{\Delta\dot{V}_2(k)}{\dot{Z}_2} \tag{7}$$

must be satisfied. If both sides of (7) are multiplied by $\dot{V}_{\text{com}}^*(k)$, an equation of powers is obtained, expressing the peer-to-peer energy transfer, where * denotes the complex conjugate. Hence, if the output powers of the network members are changed by the same amount and at the same time, they can be decoupled from the rest of the system. This superposition of a system on another is called peer-to-peer energy transfer.

III. Phasor-Based Description of a Bidirectional AC/DC Converter

A. Bidirectional AC/DC Converter as a Two-Port Network

In the previous section, only the Thevenin equivalent of each member was used to model the peer-to-peer energy transfer. However, in our system, each member is a battery, connected to the ac bus through a full-bridge ac/dc converter shown in Fig. 2. To realize a peer-to-peer energy transfer system, a phasor-based model of the converter must be derived. For this, the converter is treated as a two-port network, and the phasor model of ac/dc conversion is presented.

In Fig. 2, switches Q_1–Q_4 are controlled by pulsewidth modulation (PWM) signals and are assumed to be ideal; when the voltage v_1 of the dc-side capacitor and the current i_2 of the ac-side inductor are given, their states and the values of v_2 and i_1 in Fig. 2 are listed in Table I.

TABLE I
POSSIBLE STATES OF Q_1–Q_4, AND THE VOLTAGES AND CURRENTS IN THESE STATES

	Q_1	Q_2	Q_3	Q_4	v_2	i_1
State 1	ON	OFF	OFF	ON	v_1	i_2
State 2	OFF	ON	OFF	ON	0	0
State 3	OFF	ON	ON	OFF	$-v_1$	$-i_2$
State 4	ON	OFF	ON	OFF	0	0

The time spent in each state within the PWM period ($T_{\rm pwm}$) is denoted by τ_1, τ_2, τ_3, and τ_4. Then, the duty ratio α can be defined as

$$\alpha = \frac{\tau_1 - \tau_3}{T_{\rm pwm}}, \quad \text{where } T_{\rm pwm} = \tau_1 + \tau_2 + \tau_3 + \tau_4. \tag{8}$$

In (8), α is between -1 and 1. If the voltage v_1 of the dc-side capacitor and the current i_2 of the ac-side inductor are approximately constant over one period $T_{\rm pwm}$ of the PWM, then the relationship between the averaged voltages and currents $\bar{v}_1, \bar{v}_2, \bar{i}_1, \bar{i}_2$ can be expressed as

$$\bar{v}_2 = \alpha \bar{v}_1 \tag{9}$$

$$\bar{i}_1 = \alpha \bar{i}_2. \tag{10}$$

In (9) and (10), if the voltage and current changes are considerably slower than the frequency of the PWM signal, their relationship can be expressed as functions of time. It can be expressed in the following matrix form:

$$\begin{bmatrix} \bar{v}_2(t) \\ \bar{i}_2(t) \end{bmatrix} = \begin{bmatrix} \alpha(t) & 0 \\ 0 & 1/\alpha(t) \end{bmatrix} \begin{bmatrix} \bar{v}_1(t) \\ \bar{i}_1(t) \end{bmatrix}. \tag{11}$$

Equation (11) is the TVT equation, first introduced in [24]. The TVT is an element, similar to an ideal transformer; however, the duty ratio, which can change with time, is used instead of the turns ratio.

B. Phasor Model of the Converter

As the value of α can be changed with time, it can be set to follow the function

$$\alpha_{\rm ac}(t) = \alpha_{\rm ac}^{\rm peak} \cos(\omega t + \delta) = \alpha_{\rm ac}^{\rm peak} \Re[e^{j\delta} e^{j\omega t}] \tag{12}$$

where $\alpha^{\rm peak}$ is a value between 0 and 1, ω is the angular frequency of the ac signal, δ is the phase, j is the imaginary unit, and $\Re[\cdot]$ denotes the real part of $\cdot$. The secondary side is set as the ac side. Then, the ac current becomes

$$\bar{i}_2(t) = I_{\rm ac}^{\rm peak} \cos(\omega t + \phi). \tag{13}$$

For the dc side, values averaged over one period of the following ac signal are used:

$$I_{\rm dc} \equiv \frac{1}{T_{\rm ac}} \int_0^{T_{\rm ac}} \bar{i}_1(t) {\rm d}t. \tag{14}$$

Then, $I_{\rm dc}$ can be expressed as

$$I_{\rm dc} = \frac{1}{T_{\rm ac}} \int_0^{T_{\rm ac}} \alpha_{\rm ac}^{\rm peak} \cos(\omega t + \delta) I_{\rm ac}^{\rm peak} \cos(\omega t + \phi) {\rm d}t$$
$$= \frac{1}{2} \alpha_{\rm ac}^{\rm peak} I_{\rm ac}^{\rm peak} \cos(\delta - \phi). \tag{15}$$

Replacing the peak values with the rms values (henceforth, rms values will be used), $\alpha \equiv \alpha_{\rm ac}^{\rm peak}/\sqrt{2}$ and $I_{\rm ac} \equiv I_{\rm ac}^{\rm peak}/\sqrt{2}$; $I_{\rm dc}$ can be expressed as

$$I_{\rm dc} = \alpha I_{\rm ac} \cos(\delta - \phi) = \Re[\dot{\alpha} \dot{I}_{\rm ac}^*] \tag{16}$$

where $\dot{\alpha} \equiv \alpha e^{{\rm j}\delta}$ and $\dot{I}_{\rm ac} \equiv I_{\rm ac} e^{{\rm j}\phi}$.

Set $\dot{I}_{\rm ac}$ as the phase reference ($\phi = 0$ and $\dot{I}_{\rm ac}$ is a real number) gives

$$I_{\rm dc} = \Re[\dot{\alpha} \dot{I}_{\rm ac}^*] = \Re[\dot{\alpha}] \dot{I}_{\rm ac}. \tag{17}$$

Assuming that the dc-side voltage $\bar{v}_1(t)$ is approximately constant, the dc-side averaged voltage $V_{\rm dc}$ is defined as

$$V_{\rm dc} \equiv \frac{1}{T_{\rm ac}} \int_0^{T_{\rm ac}} \bar{v}_1(t) {\rm d}t. \tag{18}$$

Then, the ac-side voltage phasor $\dot{V}_{\rm ac}$, defined by $\bar{v}_2(t) = \Re[\dot{V}_{\rm ac} e^{{\rm j}\omega t}]$, can be expressed as

$$\dot{V}_{\rm ac} = \dot{\alpha} V_{\rm dc}. \tag{19}$$

Equations (17) and (19) express the connection between the ac and dc sides using phasors and averaged values. These values can change in discrete time k. They can be expressed in a matrix form as follows:

$$\begin{bmatrix} \dot{V}_{\rm ac}(k) \\ \dot{I}_{\rm ac}(k) \end{bmatrix} = \begin{bmatrix} \dot{\alpha}(k) & 0 \\ 0 & 1/\Re[\dot{\alpha}(k)] \end{bmatrix} \begin{bmatrix} V_{\rm dc}(k) \\ I_{\rm dc}(k) \end{bmatrix}. \tag{20}$$

As $\dot{\alpha}$ is an rms-valued phasor, its amplitude can only change between 0 and $1/\sqrt{2}$. Equation (20) expresses the ac/dc converter as a TVT, which changes its $\dot{\alpha}$ in discrete time.

C. Possible TVT-Based Linear Two Ports

In (20), a general matrix of ABCD parameters is included, where $\dot{A}$, $\dot{B}$, $\dot{C}$, and $\dot{D}$ are complex constants, as

$$\begin{bmatrix} \dot{V}_{\rm ac}(k) \\ \dot{I}_{\rm ac}(k) \end{bmatrix} = \begin{bmatrix} \dot{\alpha}(k) & 0 \\ 0 & 1/\Re[\dot{\alpha}(k)] \end{bmatrix} \begin{bmatrix} V_{\rm dc}(k) \\ I_{\rm dc}(k) \end{bmatrix}$$
$$= \begin{bmatrix} \dot{A} & \dot{B} \\ \dot{C} & \dot{D} \end{bmatrix} \begin{bmatrix} V_{\rm dc}(k) \\ I_{\rm dc}(k) \end{bmatrix}. \tag{21}$$

Then, the complex power can be expressed as

$$\dot{A}\dot{C}^* \bar{V}_1^2(k) + (\dot{A}\dot{D}^* + \dot{B}\dot{C}^*) V_{\rm dc}(k) I_{\rm dc}(k) + \dot{B}\dot{D}^* I_{\rm dc}^2(k)$$
$$= \dot{V}_{\rm ac}(k) \dot{I}_{\rm ac}^*(k). \tag{22}$$

Additionally, the power can be expressed using $\dot{\alpha}$, where $\delta = \angle\dot{\alpha}$ as follows:

$$\dot{V}_{\rm ac}(k) \dot{I}_{\rm ac}^*(k) = \frac{|\dot{\alpha}| e^{j\delta}}{|\dot{\alpha}| \cos\delta} V_{\rm dc}(k) I_{\rm dc}(k) = \frac{e^{j\delta}}{\cos\delta} V_{\rm dc}(k) I_{\rm dc}(k). \tag{23}$$

To make (22) and (23) equal, regardless of $I_{\rm dc}(k)$ and $V_{\rm dc}(k)$, $\dot{A}$, $\dot{B}$, $\dot{C}$, and $\dot{D}$ must satisfy the following conditions:

$$\dot{A}\dot{C}^* = \dot{B}\dot{D}^* = 0 \tag{24}$$

$$\dot{A}\dot{D}^* + \dot{B}\dot{C}^* = \frac{e^{j\delta}}{\cos\delta}. \tag{25}$$

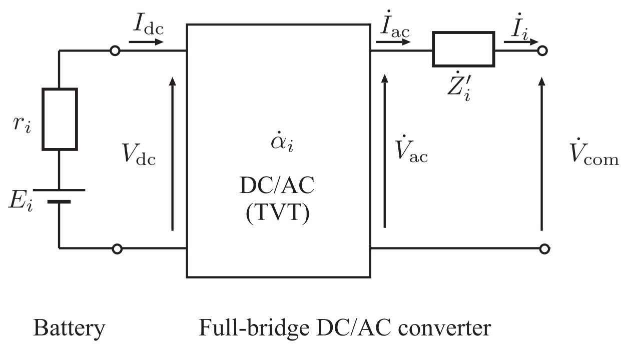

Fig. 3. Model of the converter and battery in Fig. 2. The impedance $\dot{Z}'_i$ represents the switching losses and reactive components in the ith converter $\dot{\alpha}_i$.

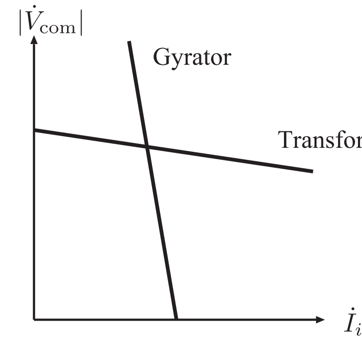

Fig. 4. Characteristics of a battery connected to a transformer and a gyrator, respectively. The gyrator case has a considerably higher slope, rendering it similar to a current source.

They have the following two possible solutions:

$$\begin{bmatrix} \dot{A} & \dot{B} \\ \dot{C} & \dot{D} \end{bmatrix} = \begin{bmatrix} \dot{A} & 0 \\ 0 & 1/\Re[\dot{A}] \end{bmatrix} \tag{26}$$

$$\begin{bmatrix} \dot{A} & \dot{B} \\ \dot{C} & \dot{D} \end{bmatrix} = \begin{bmatrix} 0 & \dot{B} \\ 1/\Re[\dot{B}] & 0 \end{bmatrix}. \tag{27}$$

As (26) is the case of a transformer with a constant duty ratio, it is a step back from the original TVT. Equation (27) exhibits a gyrator-like characteristic; hence, $\dot{B} = \dot{\beta}$ is set, where $\dot{\beta}$ is the gyrator impedance. Substituting (27) in (21), $\dot{\beta}$ can be expressed in terms of $\dot{\alpha}$ as

$$\dot{\beta} = \frac{\dot{\alpha}(k) V_{\rm dc}(k)}{I_{\rm dc}(k)}. \tag{28}$$

It is to be noted that $\angle\dot{\beta} = \angle\dot{\alpha}$. A TVT-based gyrator has already been introduced in [25]; however, it was based on a continuous-time approach, whereas ours is based on phasors.

D. Comparison of the Transformer and Gyrator

An important property of the gyrator is that it changes a connected one-port element to its dual, i.e., a capacitor is changed into a coil, as often observed in integrated circuit applications. In our case, the gyrator can be used to change the characteristics of the battery, similar to changing a voltage source into a current source. If a battery is connected to the dc side of the converter as shown in Fig. 3, and the converter operates as a transformer with a constant $\dot{\alpha}_i$ and its amplitude is limited between 0 and $1/\sqrt{2}$, the secondary-side current–voltage characteristic becomes

$$\dot{V}_{\rm com}(k) = \dot{\alpha}_i E_i - (\dot{\alpha}_i \Re[\dot{\alpha}_i] r_i + \dot{Z}'_i)\dot{I}_i(k) \tag{29}$$

where r_i is the internal resistance of the ith battery, E_i is the voltage of the ith battery, and $\dot{Z}'_i$ is the impedance, which represents the switching losses and reactive components in the ith converter. The $\dot{V}_i$ and $\dot{Z}_i$ in (1) correspond to $\dot{\alpha}_i E_i$ and $\dot{\alpha}_i \Re[\dot{\alpha}_i] r_i + \dot{Z}'_i$ in (29), respectively.

If it is operated as a gyrator, the characteristic becomes

$$\dot{V}_{\rm com}(k) = \frac{\dot{\beta}_i}{r_i} E - \left(\frac{\dot{\beta}_i \Re[\dot{\beta}_i]}{r_i} + \dot{Z}'_i \right) \dot{I}_i(k). \tag{30}$$

It is to be noted that the current phasor $\dot{I}_i$ is a real number and its sign indicates whether the battery is a source (positive) or load (negative). Assuming that the values of r_i and $|\dot{Z}'_i|$ are small, a large $|\dot{\beta}_i|$ is selected. The two characteristics of $\dot{I}_i - |\dot{V}_{\rm com}|$ in (29) and (30) for a positive, real $\dot{I}_i$ are illustrated in Fig. 4.

The purpose of peer-to-peer energy transfer is to decouple the network members from the common voltage $\dot{V}_{\rm com}$. By controlling the converters as gyrators, they can be rendered less sensitive to the changes in the common voltage. Further in the paper, it is demonstrated that the effect of the changes on the converters can be reduced with timing synchronization.

IV. Realization of a Power Gyrator for Peer-to-Peer Energy Transfer

A. Gyrator Realization by Voltage–Current Hybrid Control

It is not easy to directly use (28) to realize the gyrator because the system is discretized with at least one ac period between the sensing of the voltages and currents, and the change in $\dot{\alpha}_i$. To overcome this, voltage–current hybrid control is used, which tries to control both the voltage and current simultaneously by changing $\dot{\alpha}_i$. The feedback equation is

$$|\dot{\alpha}_i(k+1)| = |\dot{\alpha}_i(k)| + \frac{K'_i(k)}{E_i} \Big\{ \dot{V}^{\rm T}_{\rm com} - \dot{V}_{\rm com}(k) + R_{\beta i}(\dot{I}^{\rm T}_i - \dot{I}_i(k)) \Big\}. \tag{31}$$

Here, $\dot{V}^{\rm T}_{\rm com}$ is the target common voltage, $\dot{I}^{\rm T}_i$ is the target ac current of the ith module for the peer-to-peer energy transfer, and $R_{\beta i}$ is a real weight factor that decides whether the characteristic is more similar to a current or voltage source. $K'_i(k)$ is the gain and E_i is the voltage of the connected battery, used for normalizing the value in parentheses. Because the phase of $\dot{\alpha}_i(k)$ is controlled such that $\dot{V}_{\rm com}(k)$ and the currents $\dot{I}_i(k)$ have a unity power factor, it is assumed that $\dot{V}^{\rm T}_{\rm com}, \dot{I}^{\rm T}_i, \dot{V}_{\rm com}(k)$, and $\dot{I}_i(k)$ are real numbers.

If $\dot{\alpha}_i(k+1) = \dot{\alpha}_i(k)$ is set, the steady-state characteristic of hybrid control can be shown as

$$\dot{V}^{\rm SS}_{\rm com} = \dot{V}^{\rm T}_{\rm com} + R_{\beta i}\dot{I}^{\rm T} - R_{\beta i}\dot{I}^{\rm SS}_i. \tag{32}$$

In (32), $\dot{V}_{\text{com}}^{\text{T}} + R_{\beta i}\dot{I}_i^{\text{T}}$ is the V-axis intersect and $-R_{\beta i}$ is the slope. If they are set equal to the intersect and slope, respectively, of (30), a gyrator in the steady state can be approximately realized as

$$R_{\beta i} = \left|\frac{\dot{\beta}_i \Re[\dot{\beta}_i]}{r_i} + \dot{Z}_i'\right|, \quad \dot{V}_{\text{com}}^{\text{T}} + R_{\beta i}\dot{I}_i^{\text{T}} = \left|\frac{\dot{\beta}_i}{r_i}E_i\right|. \tag{33}$$

Because $\dot{\beta}_i \approx \Re[\dot{\beta}_i]$ and $|\dot{Z}_i| \ll |\dot{\beta}_i^2/r_i|$ are satisfied, $\dot{\beta}_i$ and $R_{\beta i}$ in (33) can be approximately calculated by

$$|\dot{\beta}_i| \approx \frac{E_i/\dot{I}_i^{\text{T}} + \sqrt{(E_i/\dot{I}_i^{\text{T}})^2 - 4\dot{V}_{\text{com}}^{\text{T}} r_i/\dot{I}_i^{\text{T}}}}{2}, \quad R_{\beta i} \approx \frac{\dot{\beta}_i^2}{r_i}. \tag{34}$$

As both $\dot{V}_{\text{com}}^{\text{T}}$ and $\dot{I}_i^{\text{T}}$ lie on the characteristic lines (32), they can be set as target values when realizing a gyrator with hybrid control.

B. Hybrid-Control Gain

In the previous section, the setting of the target values and weight factor of the hybrid control were explained. In this section, the gain setting for reducing the transients in the common voltage during peer-to-peer energy transfer is explained. Ideally, the convergence of the current to the target value must be described by the simple relationship

$$\dot{I}_i(k+1) - \dot{I}_i(k) = \Delta\dot{I}_i = K_i(\dot{I}_i^{\text{T}} - \dot{I}_i(k)). \tag{35}$$

If the convergence follows (35), only the value of the constant gain K_i between the two converters of the peer-to-peer energy transfer must be shared for maintaining equal currents even during transients. Hence, the relationship between $\Delta\dot{I}_i$ and $(\dot{I}_i^{\text{T}} - \dot{I}_i(k))$ is derived.

As $\dot{V}_{\text{com}}(k)$ is constant during the peer-to-peer energy transfer, this assumption is made, and the relationship between $\Delta\dot{\alpha}_i$ and $\Delta\dot{I}_i$ is derived, where $\Delta\dot{\alpha}_i = \dot{\alpha}_i(k+1) - \dot{\alpha}_i(k)$. From (29), the relationship between $\dot{\alpha}_i(k)$ and $\dot{I}_i(k)$ is as follows:

$$\dot{\alpha}_i(k)(r_i\Re[\dot{\alpha}_i(k)] + \dot{Z}_i')\dot{I}_i(k) = \dot{\alpha}_i(k)E_i - \dot{V}_{\text{com}} \tag{36}$$

and is the same for $k+1$, using $\Delta\dot{I}_i$ and $\Delta\dot{\alpha}_i$ as

$$\begin{aligned}((\dot{\alpha}_i(k) + \Delta\dot{\alpha}_i)r\Re[\dot{\alpha}_i(k) + \Delta\dot{\alpha}_i] + \dot{Z}_i')(\dot{I}_i(k) + \Delta\dot{I}_i)\\ = (\dot{\alpha}_i(k) + \Delta\dot{\alpha}_i)E_i - \dot{V}_{\text{com}}.\end{aligned} \tag{37}$$

Subtracting (36) from (37), and rearranging it to express $\Delta\dot{I}_i$ gives, (38) and (39) shown at the bottom of this page, where the approximation $\Delta\dot{\alpha}_i \ll \dot{\alpha}_i$ is used because the small changes of α_i generate large changes of $\dot{I}_i$ in the system.

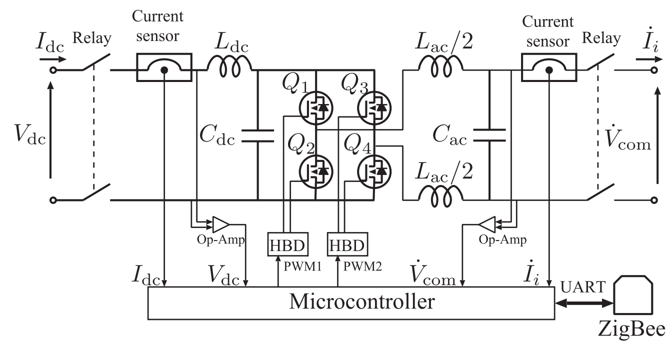

Fig. 5. Overview of the peer-to-peer energy transfer system module.

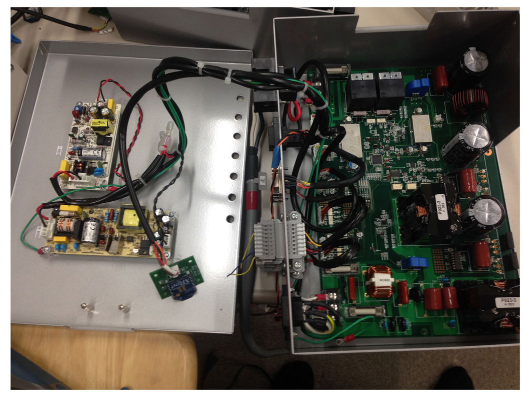

Fig. 6. Peer-to-peer energy transfer system module. The size is 315 mm × 215 mm × 110 mm and the weight is 5.7 kg.

Using approximations $\dot{\alpha}_i \approx \Re[\dot{\alpha}_i] \approx |\dot{\alpha}_i|$, $\Delta\dot{\alpha}_i \approx |\dot{\alpha}_i(k+1)| - |\dot{\alpha}_i(k)|$, $\dot{Z}_i' \approx |\dot{Z}_i'|$, and (31)

$$\begin{aligned}\Delta\dot{I}_i &\approx \frac{E_i - 2|\dot{\alpha}_i(k)|r_i\dot{I}_i(k)}{|\dot{Z}_i'| + |\dot{\alpha}_i(k)|^2 r_i}(|\dot{\alpha}_i(k+1)| - |\dot{\alpha}_i(k)|) &(40)\\ &\approx K_i' \frac{R_{\beta i}(E_i - 2|\dot{\alpha}_i(k)|r_i\dot{I}_i(k))}{E_i(|\dot{Z}_i'| + |\dot{\alpha}_i(k)|^2 r_i)}(\dot{I}_i^T - \dot{I}_i(k)). &(41)\end{aligned}$$

To make (41) similar to (35), K_i' must be set as a function of k as

$$K_i'(k) = K_i \frac{E_i(|\dot{Z}_i'| + |\dot{\alpha}_i(k)|^2 r_i)}{R_{\beta i}(E_i - 2|\dot{\alpha}_i(k)|r_i\dot{I}_i(k))}. \tag{42}$$

If $K_i'(k)$ is set to follow the above equation, the transients can be reduced during the peer-to-peer energy transfer.

$$\begin{aligned}\Delta\dot{I}_i &= \frac{\Delta\dot{\alpha}_i E_i - (\dot{\alpha}_i(k)\Re[\Delta\dot{\alpha}_i] + \Re[\dot{\alpha}_i(k)]\Delta\dot{\alpha}_i + \Delta\dot{\alpha}_i\Re[\Delta\dot{\alpha}_i])r_i\dot{I}_i(k)}{\dot{Z}_i' + \dot{\alpha}_i(k)\Re[\dot{\alpha}_i(k)]r_i + \dot{\alpha}_i(k)\Re[\Delta\dot{\alpha}_i]r_i + \Delta\dot{\alpha}_i\Re[\dot{\alpha}_i(k)]r_i + \Delta\dot{\alpha}_i\Re[\Delta\dot{\alpha}_i]r_i} &(38)\\ &\approx \frac{\Delta\dot{\alpha}_i E_i - (\dot{\alpha}_i(k)\Re[\Delta\dot{\alpha}_i] + \Re[\dot{\alpha}_i(k)]\Delta\dot{\alpha}_i)r_i\dot{I}_i(k)}{\dot{Z}_i' + \dot{\alpha}_i(k)\Re[\dot{\alpha}_i(k)]r_i} &(39)\end{aligned}$$

V. Peer-to-Peer Energy Transfer System Module

In Figs. 5 and 6, the circuit diagram of the ac/dc converter module used in our experiments is depicted. The power circuit consists of four SiC MOSFETs (Rohm SCT2080KE), which are controlled by 60-kHz PWM signals sent through half-bridge drivers (HBD, IRS21844). The capacitor and coil values are $C_{\rm dc} = 471\,\mu$F, $L_{\rm dc} = 125\,\mu$H, $C_{\rm ac} = 9.4\,\mu$F, and $L_{\rm ac} = 1.4$ mH. The ac-side outputs a 60-Hz sinusoidal wave and is implemented by a lookup table of the duty ratio $\alpha_{\rm ac}$.

The microcontroller measures the voltage and current values $\dot{V}_{\rm com}, \dot{I}_i, V_{\rm dc}, I_{\rm dc}$ with a 10-bit 60-kHz analog to digital converter, where the digital values are accumulated over $T_{\rm ac}$; the phasor amplitude of the ac values and the averaged values are calculated. The modules communicate with each other through a ZigBee wireless communication module connected through a 9600-bit/s universal asynchronous receiver/transmitter (UART). For accurate gain matching, the values of E_i and r_i must be measured. E_i is measured as the dc-side voltage when the dc-side current is zero. Then, r_i is calculated by

$$r_i = \frac{E_i - V_{\rm dc}}{I_{\rm dc}}. \tag{43}$$

Each converter output is synchronized with the common voltage. The synchronization algorithm relies on the zero-cross of the signal. The converter measures the time between the zero-crosses and sets its output period equal to the sensed period. After the frequencies are synchronized, the converter starts adjusting its own phase such that its zero-crosses match the common voltage. This adjustment is done by a simple feedback, where the time difference between the zero-crosses of the common signal and the converter is measured and the phase of the converter is adjusted to reduce this difference.

For peer-to-peer energy transfer, it is necessary to time the changes accurately. The details of our timing synchronization protocol are described in Appendix A, which is based on estimating the communication delays in the system, and is further enhanced using zero-cross sensing.

VI. Modeling and Experiments

A. Network Layout for Peer-to-Peer Energy Transfer

For the modeling and experiments, a network consisting of three network members was used, as shown in Fig. 7. Two of the converters were operated as gyrators and participated in peer-to-peer energy transfer. The module of $\dot{\alpha}_1$ is a source side and the module of $\dot{\alpha}_2$ is a load side. The module $\dot{\alpha}_2$ requests a power $P_1 = -P_2$ to the module $\dot{\alpha}_1$ and both modules change their powers from 0 to $P_1 = \dot{V}_{\rm com}\dot{I}_1^{\rm T}$ and $P_2 = \dot{V}_{\rm com}\dot{I}_2^{\rm T}$ simultaneously. The third was controlled by voltage feedback. In this case, the "rest of the network" is represented by the voltage-controlled converter. As there is only one module, it is a weak and sensitive voltage source, making the possible errors obvious. Nominal parameter values are listed in Table II. That is, the power of the transfer changes from 0 to 400 W with gain $K = 0.5$.

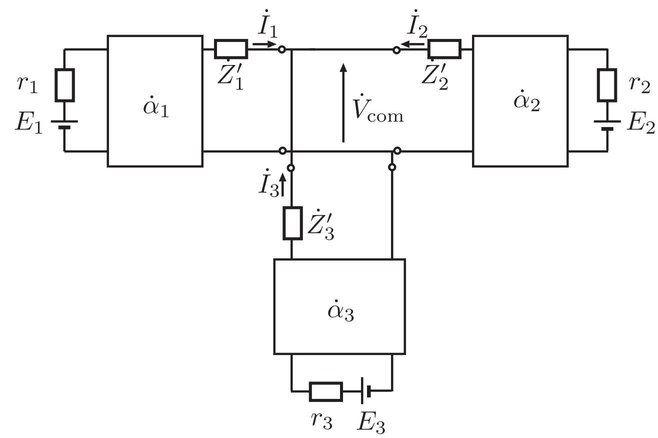

Fig. 7. Circuit used for modeling. Converters with $\dot{\alpha}_1$ and $\dot{\alpha}_2$ are participating in peer-to-peer energy transfer and are controlled by voltage–current hybrid feedback. $\dot{\alpha}_3$ is calculated using pure voltage feedback.

TABLE II
Nominal Parameter Values for the Peer-to-Peer Energy Transfer Experiments

Parameters	Values
$\dot{V}_{\rm com}^{\rm T}$	100 V
$\dot{I}^{\rm T}$	4 A
K, K_V	0.5
E_1, E_2, E_3	215 V
r_1, r_2, r_3	2.3Ω

The feedback equations are as follows:

$$|\dot{\alpha}_1(k+1)| = |\dot{\alpha}_1(k)| + \frac{K'_1(k)}{E_1}\Big\{\dot{V}_{\rm com}^{\rm T} - \dot{V}_{\rm com}(k) + R_{\beta 1}(\dot{I}_1^{\rm T} - \dot{I}_1(k))\Big\} \tag{44}$$

$$|\dot{\alpha}_2(k+1)| = |\dot{\alpha}_2(k)| + \frac{K'_2(k)}{E_2}\Big\{\dot{V}_{\rm com}^{\rm T} - \dot{V}_{\rm com}(k) + R_{\beta 2}(\dot{I}_2^{\rm T} - \dot{I}_2(k))\Big\} \tag{45}$$

$$|\dot{\alpha}_3(k+1)| = |\dot{\alpha}_3(k)| + \frac{K_V}{E_3}(\dot{V}_{\rm com}^{\rm T} - \dot{V}_{\rm com}(k)) \tag{46}$$

where $\dot{I}_1^{\rm T} = -\dot{I}_2^{\rm T} = \dot{I}^{\rm T}$.

B. Simulation for Peer-to-Peer Energy Transfer

To create a benchmark for comparing our experimental results, the network was modeled in discrete time and was implemented on MATLAB. It was assumed that $\dot{V}_{\rm com}$ and the currents were synchronized, i.e., they have a unity power factor. $\dot{\alpha}_i$ was calculated using the feedback equations (44)–(46). Using $\dot{\alpha}_i$, the voltages and currents were calculated by solving the circuit equations. The details of the calculations are provided in Appendix B. Only the simulation steps are depicted here. They are as follows:

1) The initial parameters of the model, such as E_i, r_i, and $\dot{Z}'_i$, and the initial value of $\dot{\alpha}_i(0)$ are set. Using these

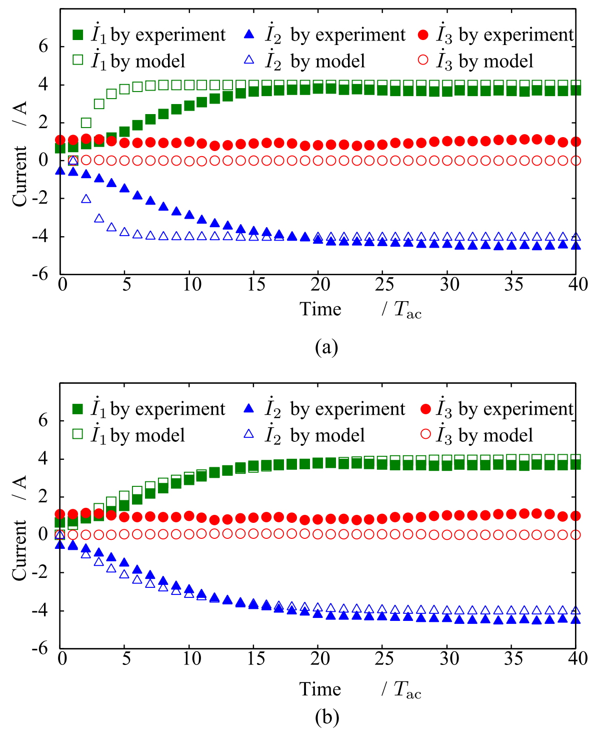

Fig. 8. Comparison of the measurement and model current results, excluding the impedances $\dot{Z}_1'$ and $\dot{Z}_2'$. The filled dots indicate the experimental results and the white dots, the calculated results by the model. (a) $\dot{Z}_1' = \dot{Z}_2' = 0\,\Omega$. As $\dot{Z}_1'$ and $\dot{Z}_2'$ were set to zero for both the model and control algorithm, the experiment and model show different results. (b) $\dot{Z}_1' = \dot{Z}_2' = 1.4 + 0.5\mathrm{j}\,\Omega$. Values of $\dot{Z}_1'$ and $\dot{Z}_2'$ are adjusted such that they match the experimental results as much as possible.

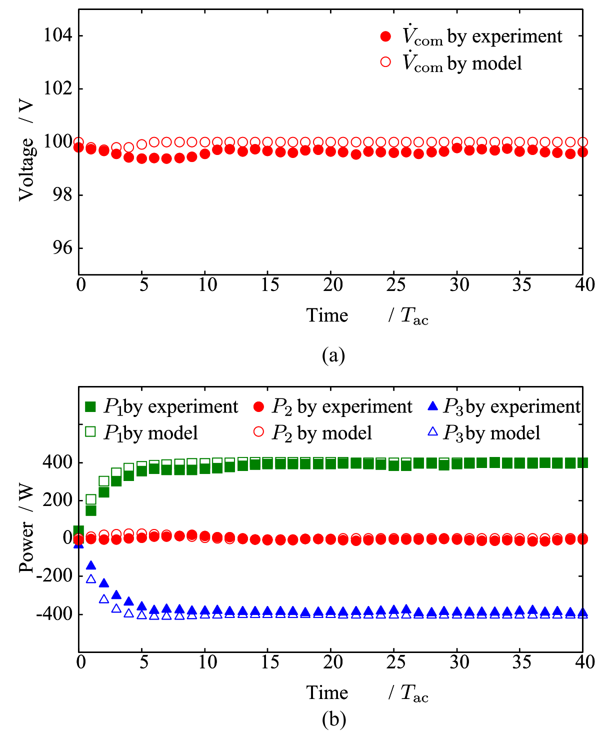

Fig. 9. Transients during successful peer-to-peer energy transfer. The voltage remains mostly unchanged because the changes in power are well balanced. (a) Voltage at the common point $\dot{V}_{\mathrm{com}}$. (b) Power of each module P_1, P_2, and P_3 defined by $\dot{V}_{\mathrm{com}}\dot{I}_1$, $\dot{V}_{\mathrm{com}}\dot{I}_2$, and $\dot{V}_{\mathrm{com}}\dot{I}_3$, respectively, because of the unity power factor. The filled dots indicate the experimental results and the white dots, the calculated results by the model.

parameters, the initial values of $\dot{I}_i(0)$ and $\dot{V}_{\mathrm{com}}(0)$ are calculated, additionally.

2) The target real values $\dot{V}_{\mathrm{com}}^{\mathrm{T}}$ and $\dot{I}^{\mathrm{T}}$ are set, and the appropriate gyrator impedance $R_{\beta i}$ is calculated by (34), for the modules participating in peer-to-peer energy transfer.
3) The new $(k+1)$ values of $|\dot{\alpha}_i|$ are calculated based on feedback equations (44)–(46).
4) Using $|\dot{\alpha}_i(k+1)|$, the values of $\dot{V}_{\mathrm{com}}(k+1)$ and $\dot{I}_i(k+1)$ are calculated.
5) Using $|\dot{\alpha}_i(k+1)|$, $\dot{V}_{\mathrm{com}}(k+1)$, and $\dot{I}_i(k+1)$, the phases of $\dot{\alpha}_i(k+1)$ are calculated.
6) Repeat steps 3)–5), a set number of times.

C. Experiment 1: Impedance Measurement

To use (42) for setting the hybrid control gain, the impedances $\dot{Z}_1'$ and $\dot{Z}_2'$ of the converters are needed. To measure this, our experimental results are compared and values that provide the closest match are selected. The results are shown in Fig. 8. In Fig. 8(a), the $\dot{Z}_1'$ and $\dot{Z}_2'$ values were set to zero for both the model and the module control algorithm, respectively. The filled dots indicate the experimental results and the white dots, the calculated results by the model. The modeling and experimental results show different values because the impedances $\dot{Z}_1'$ and $\dot{Z}_2'$ were not considered. In Fig. 8(b), the values of $\dot{Z}_1'$ and $\dot{Z}_2'$ were adjusted such that they match the experimental results as much as possible. These values were $\dot{Z}_1' = \dot{Z}_2' = 1.4 + 0.5j\,\Omega$. In the other experiments, these values were used for the model as well as the experiments.

D. Experiment 2: Peer-to-Peer Energy Transfer

In this experiment, $\dot{Z}_1'$ and $\dot{Z}_2'$ are used to calculate the gain matching of the hybrid control. The results are shown in Fig. 9, where the power P_i is defined by $P_i = \dot{I}_i\dot{V}_{\mathrm{com}}$ because the power factor equals to 1. The modeling and experimental results are close, demonstrating that the previously calculated $\dot{Z}$ is accurate. Peer-to-peer energy transfer is successful because the change in output power did not affect the common voltage considerably. The differences between the model and measurement are due to the inaccuracies in the control of the converter, such as the voltage and current measurement errors, and the low granularity of the discrete values used by the microcontroller.

E. Experiment 3: Comparison of Peer-to-Peer Energy Transfer With and Without Gain Matching

In this experiment, the importance of gain matching during peer-to-peer energy transfer is demonstrated. In the previous experiments, as the batteries were similar even without gain matching, the results may have been good; however, in these two experiments, r_1 is changed to approximately 9.0 Ω by inserting

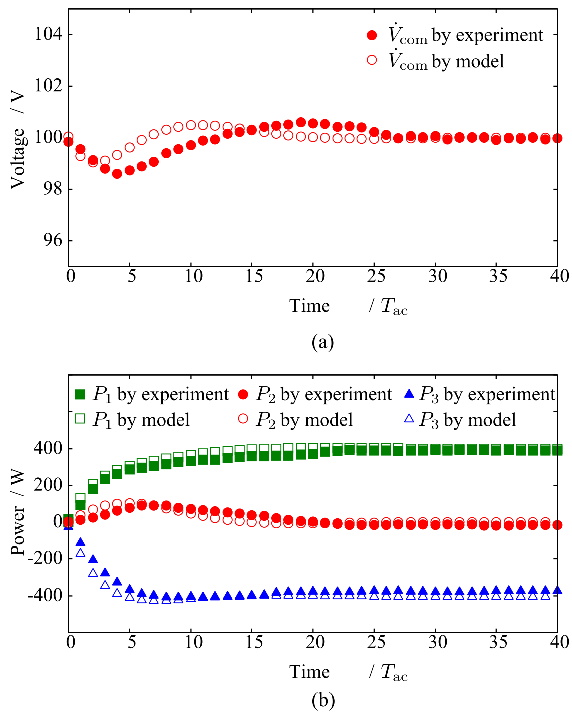

Fig. 10. Transients during peer-to-peer energy transfer, when gain matching is turned OFF. A resistor is inserted between the first module and its battery to change the resistance to 9.0Ω. As the changes between the modules are not matched, the transients are significant. (a) Voltage at the common point $\dot{V}_{\rm com}$. (b) Power of each module P_1, P_2, and P_3 defined by $\dot{V}_{\rm com}\,\dot{I}_1$, $\dot{V}_{\rm com}\,\dot{I}_2$, and $\dot{V}_{\rm com}\,\dot{I}_3$, respectively, because of the unity power factor. The filled dots indicate the experimental results and the white dots, the results calculated by the model.

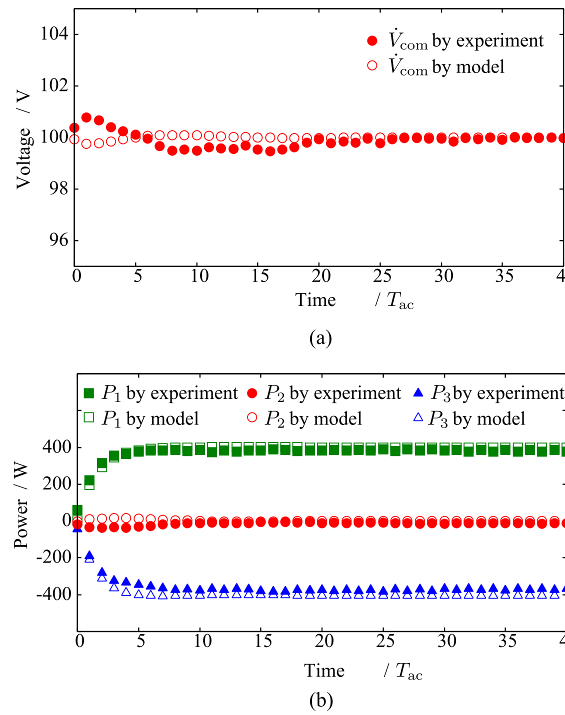

Fig. 11. Transients during peer-to-peer energy transfer with gain matching. A resistor was connected between the first converter and its battery. The transients are considerably smaller than those in Fig. 10 and can be further reduced by setting a lower gain. (a) Voltage at the common point $\dot{V}_{\rm com}$. (b) Power of each module P_1, P_2, P_3 defined by $\dot{V}_{\rm com}\,\dot{I}_1$, $\dot{V}_{\rm com}\,\dot{I}_2$, $\dot{V}_{\rm com}\,\dot{I}_3$, respectively because of the unity power factor. The filled dots indicate the experimental results and the white dots, the calculated results by the model.

a resistor between the converter and battery. Then, for the first measurement, gain matching is turned OFF; the results are shown in Fig. 10.

It can be seen that there is significant change in voltage and the output power of the voltage source, signaling that peer-to-peer energy transfer was not achieved in the beginning. In the next experiment, gain matching was turned ON. The results are shown in Fig. 11. In this case, the transients are considerably smaller. The powers are imperfectly matched as the assumption that $\Delta\dot{I}$ is small does not hold in this case because a relatively high gain of 0.5 is set. The transient can be further reduced by selecting a smaller gain; however, this would result in slower convergence.

F. Experiment 4: Peer-to-Peer Energy Transfer During Timing Desynchronization

In this experiment, the importance of timing synchronization is demonstrated. The experimental setup is similar to those used previously; however, the changes are not synchronized in time, i.e., there is a time difference of five ac periods between the changes. The results are shown in Fig. 12. The timing desynchronization caused large transients because the converters changed their outputs at different times, causing unbalance in the system. As our system is simple, the converters finally reached their target values; however, in a more complicated system, such large

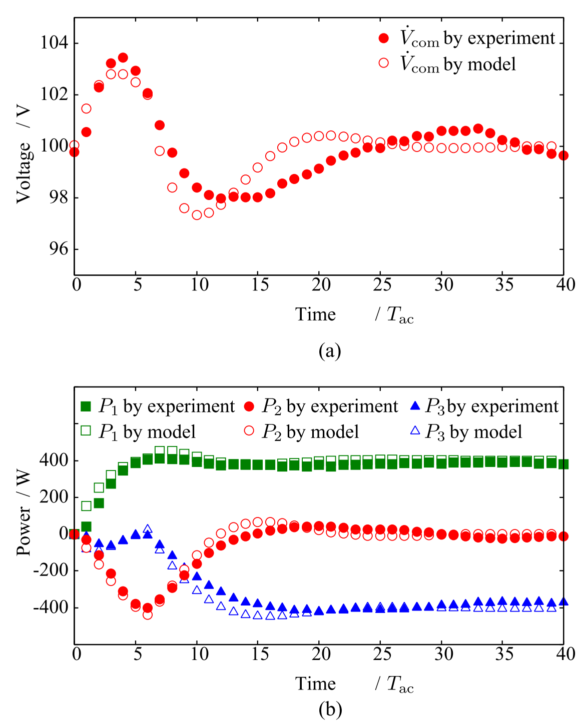

Fig. 12. Transients during timing desynchronization. There is a five-ac-period time difference between the two modules. The transients are large, indicating the imbalance in the system. (a) Voltage at the common point $\dot{V}_{\rm com}$. (b) Power of each module P_1, P_2, and P_3 defined by $\dot{V}_{\rm com}\,\dot{I}_1$, $\dot{V}_{\rm com}\,\dot{I}_2$, and $\dot{V}_{\rm com}\,\dot{I}_3$, respectively because of the unity power factor. The filled dots indicate the experimental results and the white dots, the calculated results by the model.

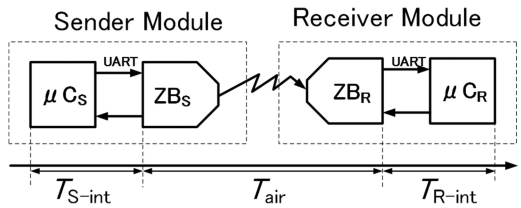

Fig. 13. Communication delay between two modules can be divided into three parts: the internal delay in the sender module ($T_{\text{S-int}}$), the travel time between the two modules (T_{air}), and the internal delay in the receiver module ($T_{\text{R-int}}$).

transients might cause some of the system elements to break down.

VII. Conclusion

A peer-to-peer energy transfer system was introduced, in which two network members match their changes in the order of milliseconds, for decoupling the power network from the common bus. A phasor-based model of the bidirectional ac/dc converter was formulated as a two-port representation, and used for deriving a gyrator using the TVT concept. It was demonstrated that the gyrator can be realized in the steady state using voltage–current hybrid control, and a gain-matching method was proposed for the transients of the peer-to-peer energy transfer.

In addition, a timing synchronization protocol was introduced for peer-to-peer energy transfer communication, based on the estimation of the communication delays between the members of the network. The transients of the peer-to-peer energy transfer were modeled and compared with the experimental results. From these results, the possibility of peer-to-peer energy transfer was confirmed.

Appendix A
Timing-Synchronization Protocol

A. Constituents of the Communication Delay Between Two Modules

The communication delay between two modules can be divided into three parts, as shown in Fig. 13.

1) $T_{\text{S-int}}$ is the time taken to generate a message in the sender-module microcontroller (μC_S) and send it to the ZigBee module (ZB_S) through a UART. This delay time can be measured during design and saved as a constant.
2) $T_{\text{R-int}}$ is the time to transfer the message from the ZigBee (ZB_R) to the microcontroller (μC_R), decode, and act on it. This delay time can be measured during design and saved as a constant.
3) T_{air} is the time between $T_{\text{S-int}}$ and $T_{\text{R-int}}$, which includes message modulation, wireless transfer, and demodulation. As this time depends upon the distance between the modules, the models of the ZigBee modules, etc., it must be estimated for each message.

B. Protocol for Timing Synchronization

To accurately synchronize the timing of the two modules, the communication delay between them is estimated. As every module in the system is synchronized to the same ac signal, the zero-cross of the ac signal is used to improve accuracy. The timing-synchronization protocol is shown in Fig. 14.

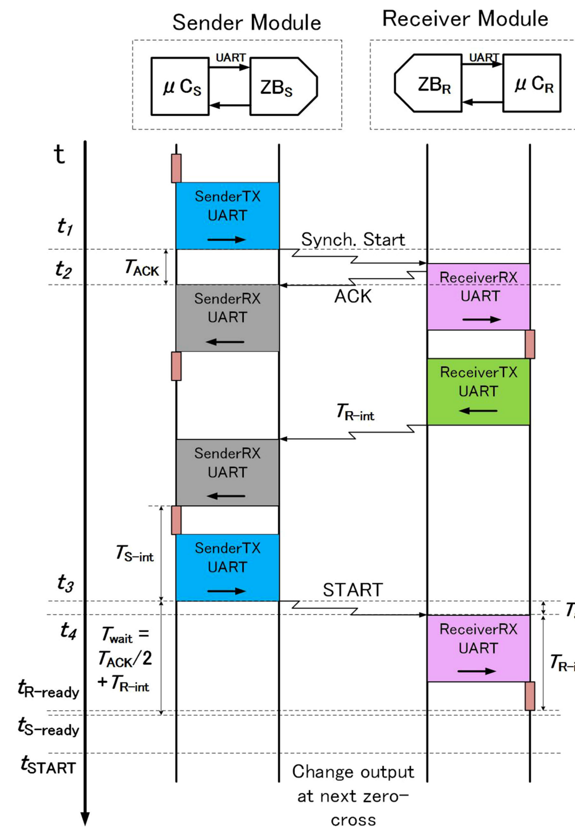

Fig. 14. Synchronization protocol. The modules communicate for estimating the communication delay between them. When the protocol is in certain states, the signals are high, as shown in Fig. 15.

1) The sender module generates a synchronization-start order and transfers it through a UART. At time t_1 the UART transfer is complete and the sender microcontroller starts a timer. ZB_S sends a message, which has an acknowledge (ACK) request, causing ZB_R to send back an ACK message, without communicating with its microcontroller.
2) At t_2, ZB_S receives the ACK, and when the first byte is transferred through the UART to μC_S, it stops its timer. The value of timer T_{ACK} is used to estimate T_{air} because $T_{\text{ACK}} \approx 2T_{\text{air}}$.
3) After μC_R receives the synchronization-start order, it sends its own internal delay $T_{\text{R-int}}$ to the sender module.
4) When μC_S receives $T_{\text{R-int}}$, it calculates the delay and sends the start order such that it arrives approximately at a minus-to-plus zero-cross [t_{goal}, as shown in Fig. 15(b)].
5) From t_3, when the transfer of the message through the UART is complete, the sender module waits for $T_{\text{wait}} = T_{\text{R-int}} + T_{\text{ACK}}/2$. At $t_{\text{S-ready}}$, it switches to a standby state waiting for the next minus-to-plus zero-cross.
6) When μC_R receives and deciphers the start order at $t_{\text{R-ready}}$, it starts waiting for the next plus-to-minus zero-cross.
7) At the next plus-to-minus zero-cross, both modules change their output simultaneously.

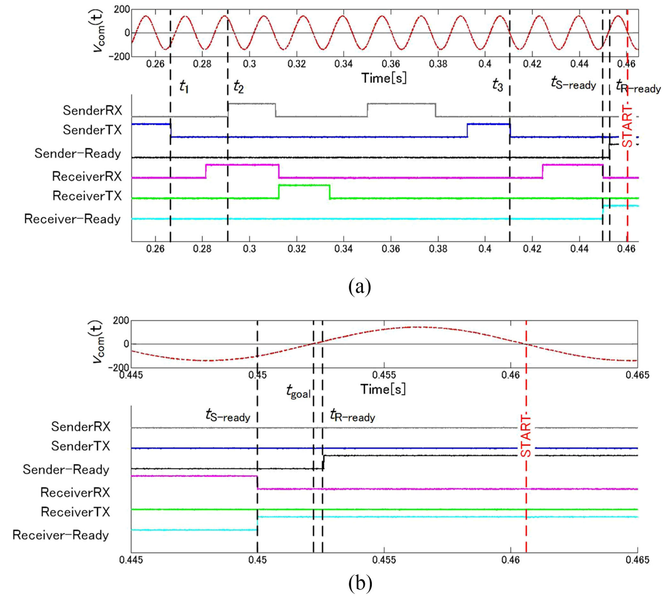

Fig. 15. Communication flow during the timing synchronization protocol, compared to the timescale of the ac voltage. A high level indicates that the signal is active. The timing synchronization protocol completes in approximately 180 ms and the timing difference is approximately 2.4 ms. (a) Overview. (b) Expansion around $t_{\text{R-ready}}$ and $t_{\text{S-ready}}$

The experimental results are shown in Fig. 15. Using the protocol, the changes were timed, in the order of milliseconds. Using the zero-cross of the common voltage, the timing difference was several microseconds.

Appendix B
Modeling Details

In our model, the power factor at the common point is unity, implying that the phases of the currents and $\dot{V}_{\text{com}}$ are all zero. Then, the relationship between $\dot{V}_{\text{com}}$ and $\dot{I}_i$ can be expressed as follows:

$$\dot{V}_{\text{com}} = \dot{\alpha}_i E_i - (\dot{\alpha}_i \Re(\dot{\alpha}_i) r_i + \dot{Z}_i')\dot{I}_i(k), \quad \text{where} \quad i = 1, 2, 3. \tag{47}$$

These equations can be written separately for the real and imaginary parts as

$$\dot{V}_{\text{com}} = \Re(\dot{\alpha}_i)E_i - (\Re(\dot{\alpha}_i)^2 r_i + \Re[\dot{Z}_i'])\dot{I}_i \tag{48}$$

$$0 = \Im(\dot{\alpha}_i)E_i - (\Im(\dot{\alpha}_i)\Re(\dot{\alpha}_i) r_i + \Im[\dot{Z}_i'])\dot{I}_i. \tag{49}$$

Equations (48) and (49) are solved and substituted in

$$|\dot{\alpha_i}|^2 = \Im(\dot{\alpha}_i)^2 + \Re(\dot{\alpha}_i)^2. \tag{50}$$

Using a symbolic math package, it is rearranged into the following equation, such that I_i is expressed as a function of $\dot{V}_{\text{com}}$:

$$p_{i4}\dot{I}_i^4 + p_{i3}\dot{I}_i^3 + p_{i2}\dot{I}_i^2 + p_{i1}\dot{I}_i^1 + p_{i0} = 0 \tag{51}$$

$$p_{i4} = |\dot{\alpha_i}|^4 r_i^2 \Re[\dot{Z}_i']^2 + 2|\dot{\alpha_i}|^2 r_i \Re[\dot{Z}_i']^3 + 2|\dot{\alpha_i}|^2 r_i \Re[\dot{Z}_i']\Im[\dot{Z}_i']^2 + \Re[\dot{Z}_i']^4 + 2\Re[\dot{Z}_i']^2\Im[\dot{Z}_i']^2 + \Im[\dot{Z}_i']^4 \tag{52}$$

$$p_{i3} = 2|\dot{\alpha_i}|^4 r_i^2 \Re[\dot{Z}_i']\dot{V}_{\text{com}} + 6|\dot{\alpha_i}|^2 r_i \Re[\dot{Z}_i']^2 \dot{V}_{\text{com}} + 2|\dot{\alpha_i}|^2 r_i \Im[\dot{Z}_i']^2 \dot{V}_{\text{com}} + 4\Re[\dot{Z}_i']^3 \dot{V}_{\text{com}} + 4\Re[\dot{Z}_i']\Im[\dot{Z}_i']^2 \dot{V}_{\text{com}} \tag{53}$$

$$p_{i2} = |\dot{\alpha_i}|^4 r_i^2 \dot{V}_{\text{com}}^2 - |\dot{\alpha_i}|^2 \Re[\dot{Z}_i']^2 E_i^2 - |\dot{\alpha_i}|^2 \Im[\dot{Z}_i']^2 E_i^2 + 6|\dot{\alpha_i}|^2 r_i \Re[\dot{Z}_i']\dot{V}_{\text{com}}^2 + 6\Re[\dot{Z}_i']^2 \dot{V}_{\text{com}}^2 + 2\Im[\dot{Z}_i']^2 \dot{V}_{\text{com}}^2 \tag{54}$$

$$p_{i1} = -2|\dot{\alpha_i}|^2 \Re[\dot{Z}_i'] E_i^2 \dot{V}_{\text{com}} + 2|\dot{\alpha_i}|^2 r_i \dot{V}_{\text{com}}^3 + 4\Re[\dot{Z}_i']\dot{V}_{\text{com}}^3 \tag{55}$$

$$p_{i0} = -|\dot{\alpha_i}|^2 E_i^2 \dot{V}_{\text{com}}^2 + \dot{V}_{\text{com}}^4. \tag{56}$$

Solving (51) for I_i, four roots for each $\dot{I}$ are obtained. An expression is obtained, where the only unknown is $\dot{V}_{\text{com}}$ by using the following:

$$\dot{I}_1 + \dot{I}_2 + \dot{I}_3 = 0. \tag{57}$$

Equation (57) is solved using a numerical solver function for every combination of $\dot{I}_i$ roots. To select the correct root, the resulting $\dot{V}_{\text{com}}$ value is substituted into (51) and a solution where every $\dot{I}_i$ and $\dot{V}_{\text{com}}$ has a real component only, and $\dot{V}_{\text{com}}$ is nonzero is selected. There is only one such solution.

References

[1] N. Hatziargyriou, H. Asano, R. Iravani, and C. Marnay, "Microgrids," *IEEE Power Energy Mag.*, vol. 5, no. 4, pp. 78–94, Jul. 2007.

[2] Y. Han, H. Li, P. Shen, E. A. A. Coelho, and J. M. Guerrero, "Review of active and reactive power sharing strategies in hierarchical controlled microgrids," *IEEE Trans. Power Electron.*, vol. 32, no. 3, pp. 2427–2451, Mar. 2017.

[3] M. C. Chandorkar, D. M. Divan, and R. Adapa, "Control of parallel connected inverters in standalone AC supply systems," *IEEE Trans. Ind. Appl.*, vol. 29, no. 1, pp. 136–143, Jan. 1993.

[4] A. Mehrizi-Sani, A. H. Etemadi, D. E. Olivares, and R. Iravani, "Trends in microgrid control," *IEEE Trans. Smart Grid*, vol. 5, no. 4, pp. 1905–1919, May 2014.

[5] J. M. Guerrero, J. Matas, L. G. de Vicuna, M. Castilla, and J. Miret, "Decentralized control for parallel operation of distributed generation inverters using resistive output impedance," *IEEE Trans. Ind. Electron.*, vol. 54, no. 2, pp. 994–1004, Apr. 2007.

[6] J. M. Guerrero, L. G. de Vicuna, J. Matas, M. Castilla, and J. Miret, "Output impedance design of parallel-connected UPS inverters with wireless load-sharing control," *IEEE Trans. Ind. Electron.*, vol. 52, no. 4, pp. 1126–1135, Aug. 2005.

[7] Y. Li and Y. W. Li, "Power management of inverter interfaced autonomous microgrid based on virtual frequency-voltage frame," *IEEE Trans. Smart Grid*, vol. 2, no. 1, pp. 33–40, Mar. 2011.

[8] T. Shintai, Y. Miura, and T. Ise, "Oscillation damping of a distributed generator using a virtual synchronous generator," *IEEE Trans. Power Del.*, vol. 29, no. 2, pp. 668–676, Apr. 2014.

[9] H. G. Xial, A. Luo, Z. K. Shuai, G. B. Jin, and Y. Huang, "An improved control method for multiple bidirectional power converters in hybrid AC/DC migrogrid," *IEEE Trans. Smart Grid*, vol. 7, no. 1, pp. 340–347, Jan. 2016.

[10] J. A. P. Lopes, C. L. Moreira, and A. G. Madureira, "Defining control strategies for microgrids in islanded operation," *IEEE Trans. Power Syst.*, vol. 21, no. 2, pp. 916–924, May 2006.

[11] J. He and Y. W. Li, "An enhanced load demand sharing strategy," *IEEE Trans. Power Electron.*, vol. 27, no. 9, pp. 1149–1158, May 2014.

[12] Y. W. Li and C. N. Kao, "An accurate power control strategy for power-electronics-interfaced distributed generation units operating in a low-voltage multibus microgrid," *IEEE Trans. Power Electron.*, vol. 24, no. 12, pp. 2977–2988, Dec. 2009.

[13] J. He, Y. W. Li, and F. Blaabjerg, "An enhanced islanding microgrid reactive power, imbalance power and harmonic power sharing scheme," *IEEE Trans. Smart Grid*, vol. 5, no. 4, pp. 1905–1919, May 2014.

[14] T. L. Lee and P. T. Cheng, "Design of a new cooperative harmonic filtering strategy for distributed generation interface converters in an islanding network," *IEEE Trans. Power Electron.*, vol. 22, no. 5, pp. 661–673, May 2014.

[15] B. B. Johnson, S. V. Dhople, A. O. Hamadeh, and P. T. Krein, "Synchronization of parallel single-phase inverters with virtual oscillator control," *IEEE Trans. Power Electron.*, vol. 29, no. 11, pp. 6124–6138, Nov. 2014.

[16] V. Nasirian, Q. Shafiee, J. M. Guerrero, F. L. Lewis, and A. Davoudi, "Droop-free distributed control for AC microgrids," *IEEE Trans. Power Electron.*, vol. 31, no. 2, pp. 1600–1617, Feb. 2016.

[17] S. Liu, X. Wang, and P. X. Liu, "Impact of communication delays on secondary frequency control in an islanded microgrid," *IEEE Trans. Ind. Electron.*, vol. 62, no. 4, pp. 2021–2031, Apr. 2015.

[18] H. Liang, B. J. Choi, W. Zhuang, and X. Shen, "Stability enhancement of decentralized inverter control through wireless communications in microgrids," *IEEE Trans. Smart Grid*, vol. 4, no. 1, pp. 321–331, Mar. 2013.

[19] B. Chaudhuri, R. Majumber, and B. C. Pal, "Wide-area measurement-based stabilizing control of power system considering signal transmission delay," *IEEE Trans. Power Syst.*, vol. 19, no. 4, pp. 1971–1979, Nov. 2004.

[20] S. Ci, J. Qian, D. Wu, and A. Keyhani, "Impact of wireless communication delays on load sharing among distributed generation systems through smart microgrids," *IEEE Wireless Commun.*, vol. 19, no. 3, pp. 24–29, Jun. 2012.

[21] C. Ahumada, R. Cárdenas, D. Sáez, and J. M. Guerrero, "Secondary control strategies for frequency restoration in islanded microgrids with consideration of communication delay," *IEEE Trans. Smart Grid*, vol. 7, no. 3, pp. 1430–1441, May 2016.

[22] C. Dou, D. Yue, Z. Zhang, and J. M. Guerrero, "Hierarchical delay-dependent distributed coordinated control for DC ring-bus microgrids," *IEEE Access*, vol. 5, pp. 10130–10140, Jun. 2017.

[23] H. Behjati, A. Davoudi, and F. Lewis, "Modular DC–DC converters on graphs: Cooperative control," *IEEE Trans. Power Electron.*, vol. 29, no. 12, pp. 6725–6741, Dec. 2014.

[24] B. D. Anderson, D. A. Spaulding, and R. W. Newcomb, "The time-variable transformer," *Proc. IEEE*, vol. 53, no. 6, pp. 634–635, Jun. 1965.

[25] S. Singer, "Loss-free gyrator realization," *IEEE Trans. Circuits Syst.*, vol. 35, no. 1, pp. 26–34, Jan. 1988.

[26] K. Mahabir, G. Verghese, V. J. Thottuvelli, and A. Heyman, "Linear averaged and sampled data models for large signal control of high power factor AC–DC converters," in *Proc. 21st Annu. Conf. Power Electron. Specialists*, 1990, pp. 372–381.

[27] J. Chavarria, D. Biel, F. Guinjoan, C. Meza, and J. J. Negroni, "Energy balance control of PV cascaded multilevel grid-connected inverters under level-shifted and phase-shifted PWMs," *IEEE Trans. Ind. Electron.*, vol. 60, no. 1, pp. 98–111, Jan. 2013.

Daniel Kiss received the B.E. and M.E. degrees in electrical engineering from Kyoto University, Kyoto, Japan, in 2015 and 2017, respectively.

His research interests include the analysis and design of complex systems and power flow control.

Takashi Hisakado received the B.E. and M.E. degrees in electrical engineering II and the Dr. Eng. degree in electrical engineering from Kyoto University, Kyoto, Japan, in 1993, 1995, and 1997, respectively.

He is currently an Associate Professor with the Department of Electrical Engineering, Kyoto University. His research interests include the design of electromagnetic phenomena and power flows.

Dr. Hisakado is a member of the Institute of Electronics, Information and Communication Engineers of Japan and the Institute of Electrical Engineers of Japan.

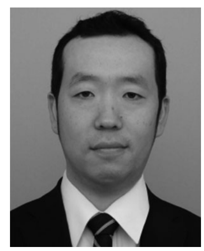

Tohlu Matsushima received the M.E. and Ph.D. degrees in communication network engineering from Okayama University, Okayama, Japan, in 2006 and 2009, respectively.

Since 2009, he has been an Assistant Professor with the Department of Electrical Engineering, Kyoto University, Kyoto, Japan. In 2018, he became an Associate Professor with the Department of Electrical and Electronic Engineering, Kyushu Institute of Technology, Kitakyushu, Japan. His research interest includes the electromagnetic interference problem.

Dr. Matsushima is a member of the Institute of Electronics, Information and Communication Engineers, the Institute of Electrical Engineers of Japan, and the Japan Institute of Electronics Packaging.

Osami Wada received the B.E., M.E., and Dr. Eng. degrees in electronics from Kyoto University, Kyoto, Japan, in 1981, 1983, and 1987, respectively.

From 1988 to 2005, he was with the Faculty of Engineering, Okayama University, Okayama, Japan. In 2005, he became a Full Professor with the Department of Electrical Engineering, Kyoto University. His research interests include the study of the electromagnetic compatibility (EMC) of electronic circuits and systems and the development of EMC macro models of integrated circuits.

Prof. Wada was the Chair of IEEE EMC Society Japan Chapter from 2012 to 2013, and he is currently the Chair of the Technical Committee of EMC (EMCJ) at the Institute of Electronics, Information and Communication Engineers of Japan (IEICE). He is a fellow of IEICE, and a member of the Institute of Electrical Engineers of Japan and the Japan Institute of Electronics Packaging.